

Stress Concentration Factor of Expanded Aluminum Tubes Using Finite Element Modeling

L Mhamdia, AC Seibi^a, A Karrech^c, S El-Borgi^a and I Barsoum^b

^aMechanical Engineering Department, Tunisia Polytechnic School, Tunis, Tunisia

^bMechanical Engineering Program, Petroleum Institute, Abu Dhabi, United Arab Emirates

^cSchool of Civil and Resources Engineering, The University of Western Australia, Australia

Received 23 May 2012 ; accepted 31 October 2012

Abstract: This paper discusses the development of semi-empirical relations for the maximum stress concentration factor (SCF) around circular holes embedded in aluminum tubes under various expansion ratios and mandrel angles. Finite element models were developed to study the expansion of a typical aluminum tube with embedded holes of various sizes. An elastic perfectly-plastic material behaviour was used to describe the structural response of the tubes under expansion. Various hole-diameter-to-tube-wall-thickness ratios, tube expansion ratios, and mandrel angles were considered to determine the stress state around the hole at zero and 90 degree locations from which the maximum SCF was determined. Semi-empirical relations for the maximum SCF using the Lagrange interpolation formulation were developed. The developed relations were found to predict the SCFs accurately.

Keywords: Stress concentration factor, Expansion process, Semi-empirical formulations, Tube expansion

نمذجة عامل تركيز الإجهاد في أنابيب الألمنيوم الممددة باستخدام طريقة العنصر المحدود

لسعد محمدي^أ، عبد النور س سبيبي^ب، علي كرش^ج، سامي البرجي^أ و عماد برسوم^ب

الملخص: تناقش هذه الورقة تناقش علاقات شبه تجريبية لعامل تركيز الإجهاد الأقصى المتكون حول الثقوب الدائرية المضمنة في أنابيب الألمنيوم تحت تأثير عاملين أساسيين يتمثلان في نسبة تمديد الأنبوب وزوايا الجسم المغزلي المستخدم في عملية التمديد. إذ تم تطوير نموذج باستخدام طريقة العنصر المحدود بهدف دراسة عملية تمديد أنبوب ألومنيوم قياسي يحتوي على ثقوب ذات أحجام مختلفة. وقد تم استخدام سلوك المرونة المتبوع بسلوك الصلابة المتالي من أجل توصيف الاستجابة الهيكلية للأنابيب تحت تأثير عملية التمديد. كما أخذ بعين الاعتبار اختلاف نسب أقطار الحفر إلى سماكة جدار الأنبوب، واختلاف نسب التمديد للأنبوب، بالإضافة إلى استخدام زوايا مختلفة للجسم المغزلي في تحديد حالة الإجهاد حول الثقب عند زوايا صفر و ٩٠ درجة من المواقع التي تم تحديد أقصى تركيز لعامل الإجهاد عندها. وبناء على ذلك تم وضع علاقات شبه تجريبية لعامل تركيز الإجهاد الأقصى عن طريق توليد قيم المعامل باستخدام طريقة لاغرانج. وقد وجد بأن العلاقات التي تم إيجادها قادرة على التنبؤ بعامل تركيز الإجهاد بدقة.

المفردات المفتاحية: عامل تركيز الإجهاد، عملية التمديد، صياغات شبه تجريبية، تمديد الأنابيب.

1. Introduction

Solid expandable tubular technology was introduced to the oil industry in the early nineties with the aim of achieving mono-diameter wells as alternatives to existing telescopic well configurations. This led to tremendous savings of as much as 50% of the original cost of the telescopic well configurations.

This technology subjects solid tubes and sand control screens to large radial plastic deformations through expansion. The expansion process is usually performed either mechanically or hydraulically using conical mandrels. Tubular (casing) expansion has been performed down hole for well rehabilitation to repair damaged zones, corroded casing sections, and shut-off perforations. In addition, expansion of sand control

*Corresponding author's e-mail: aseibi@pi.ac.ae

screens has become a normal practice used by field engineers to increase productivity by enlarging the cross-sectional area. Sand control screens, which are generally used in horizontal wells, consist of tubes possessing slots ranging from fine at the outer surface to considerably larger-sized holes at the base plate.

The presence of holes can be problematic and presents a source of stress concentration. This may reveal some weaknesses in the structure, especially when expanded to higher expansion ratios. Chitwood *et al.* (2005) showed that a perforated 13Cr base tubular fractured after 25% expansion and cracks propagated between the perforations, causing a loss of structural integrity. Pilkey 1997 and Toubal *et al.* 2004 studied the problem of stress concentration around holes in flat plates under axial loading. Similarly, (Van Dyke 1965; Tan 1994) studied pressure vessels and their related components under internal pressure and/or axial loading. Steele *et al.* 1986 and Xue *et al.* 1991 developed an efficient numerical algorithm to determine stress variations in cylindrical vessels with large openings. Subsequently, Dennis and Palazotto 1990 extended the approach to composite structures with cut-outs. However, according to the knowledge of the authors, stress concentration around holes in expanded tubes has never been studied before. Therefore, the present work, which deals with the estimation of stress concentration around holes in expanded tubes, is the first of its kind. This work is complex in nature and represents a moving boundary problem in terms of mandrel motion within the tube passing by the embedded hole while expanding the tube to a prescribed expansion ratio. The stress concentration may induce crack initiation at the notch root which can result in loss of integrity. For this reason, the tangential stress at zero and 90 degree locations around the hole received great attention through the conduct of a finite-element analysis from which SCFs based on the maximum stress were determined.

2. Finite Element Modeling

Finite element analysis was performed on solid tubes subjected to various expansion ratios, mandrel angles, and hole-diameter-to-tube-wall thickness ratios.

Tubular expansion occurs when the mandrel moves downward and expands the solid tube to a defined expansion ratio $(D_o - D_i)/D_i * 100$ (Fig. 1). Figure 1a shows the geometrical model of a tube with an inner diameter of $D_i = 54.6$ mm, a wall thickness of $t = 6$ mm, and an embedded circular hole of variable diameter, d . The figure also shows a conical mandrel with mandrel angle β and an outer diameter of D_o , which

can be varied according to expansion requirements. Points 1 and 2 are located at zero and 90 degree positions around the hole and are the focus of this study, where the variations of the tangential stress at both locations were taken as the mandrel moves downward to expand the tube. This expansion process subjects the tube to a compression state ahead of the mandrel, due to the end conditions. A three-dimensional brick element and an analytic rigid body element were used to model the tube and mandrel, respectively, as shown in Fig. 1b. The mandrel/tube interaction was modeled using a Coulomb friction model where a friction coefficient of 0.1 was used.

Proper boundary conditions representative of lab and field conditions are essential to obtaining accurate results. Special attention must be focused on the region in the vicinity of the hole where stress concentration occurs. The zoomed window section in Fig. 1b shows the finite element mesh of the tube where fine meshes were used in the vicinity of the hole due to the high stress concentration experienced during expansion in this region. An elastic perfectly-plastic material model was used to describe the tube's behaviour. The material properties used for the tube were elastic modulus $E = 67$ GPa, Poisson's ratio $\nu = 0.3$, and tensile yield stress $\sigma_y = 150$ MPa. Tube expansion in this study was performed by constraining all nodes lying at the bottom side of the tube from moving in any direction, whereas all other nodes were free to move. Since the mandrel was modeled as a rigid body, a vertical downward displacement was given to its reference point, which was located along its centre line at the top face to move the mandrel down.

3. Case Study

In this study, the friction coefficient was taken as 0.1 for the entire finite element analysis. Three mandrel angles of $\beta = 10, 22.5, \text{ and } 30^\circ$, as well as five expansion ratios of $e = 5, 10, 15, 20, \text{ and } 25\%$ were used. In addition, eight hole-diameter-to-tube-wall-thickness ratios were used: $d/t = 0.1, 0.2, 0.6, 0.8, 1.0, 1.2, \text{ and } 1.5$. The tangential stress of zero and 90 degrees was taken from the finite element results from which the nominal and peak stress values were computed. The generated data were used to determine the maximum SCF at both locations. Peak values of the tangential stress were used to estimate the SCF defined by Chitwood *et al.* (2005) as:

$$K_{\max(\theta=0,90)} = \frac{\sigma_{\max}(x)|_{(0,90)}}{\sigma_{ave}} \quad (1)$$

$$\sigma_{ave} = \frac{1}{L} \int_0^L \sigma(x) dx$$

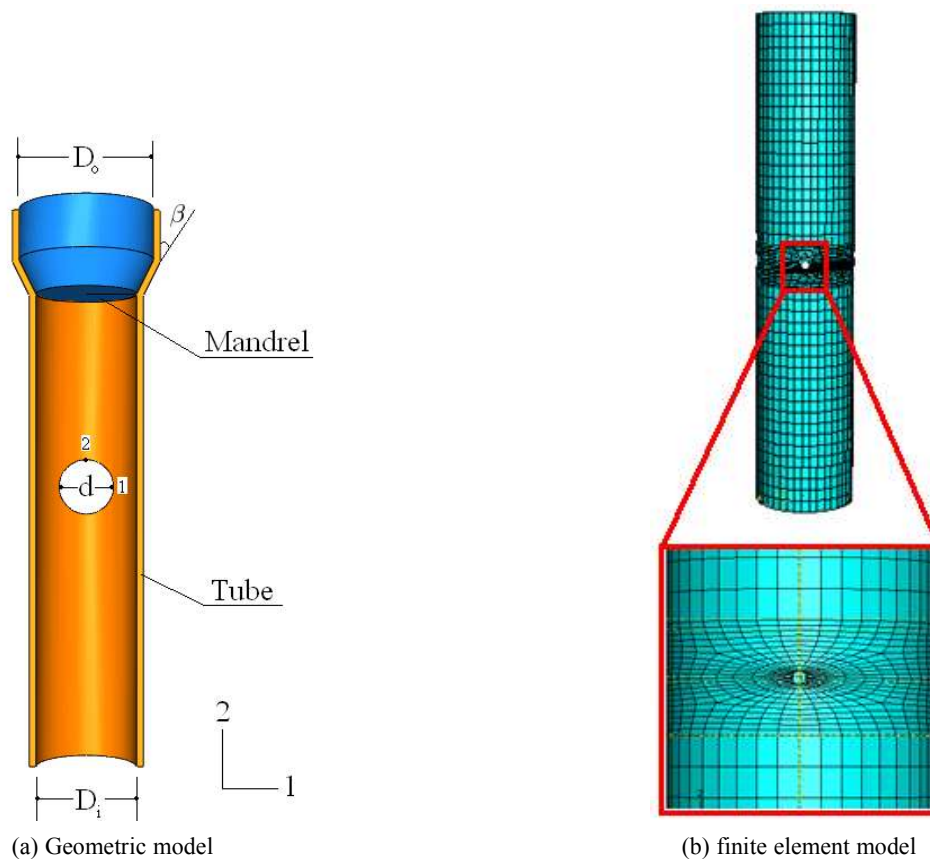


Figure 1. Geometric and finite element models of the tubular expansion process

where $\sigma_{max}(x)|_{(0,90)}$ is the maximum stress at zero and 90 degrees, and x denotes the mandrel position along the tube during the expansion process. The stress σ_{ave} is defined as the average stress of the stress variation before the mandrel reaches the hole. It is worth noting that Eqn. (1) differs from the traditional definition of the stress concentration where the nominal stress is taken into account instead of the average stress used in this study.

4. Results and Discussions

The finite element results focus on the stress state at zero and 90 degrees at locations around the hole from which the maximum SCF can be determined. Figure 2 shows the variation of the drawing force as a function of the mandrel position for various expansion ratios and mandrel angles. In all cases, the figure shows that the force increases with an increase in expansion ratio and mandrel angle. Figure 2d shows a summary of the average drawing force in terms of expansion ratio for three mandrel angles, indicating that the force increases with an increase in both expansion ratio and mandrel angle.

Typical stress variations of σ_{22} and σ_{11} in terms of

mandrel position are shown in Figs. 3 and 4. It is worth noting that the tangential stress at points 1 and 2 are respectively compressive and tensile when the mandrel is far away from the hole, since tube expansion was performed under compression. The two stresses become more compressive as the mandrel approaches the hole and changes sign to become tensile, reaching peak values while expanding the hole. As the mandrel passes the expanded hole, residual compressive stresses were induced at both locations. This behavior is shown in Fig. 5 where the shape variation of the hole during the three stages of expansion is clearly observed. It can be seen that the hole is under compressive and tensile stress state at points 1 and 2, respectively, when the mandrel is far away from the hole. As the mandrel approaches the hole and starts expanding the region in the vicinity of the hole, the hole becomes oval (Fig. 5b) and the stress state at both locations becomes tensile due to the hole's enlargement. As the mandrel passes the expanded zone of the hole, the hole tends to recover; therefore, the residual stress becomes compressive at both locations. Peak values of σ_{11} and σ_{22} were used to compute the maximum $K_{max(0,90)}$ at points 1 and 2 in terms of a hole-diameter-to-tube-wall-thickness ratio as well as mandrel angle and expansion ratio.

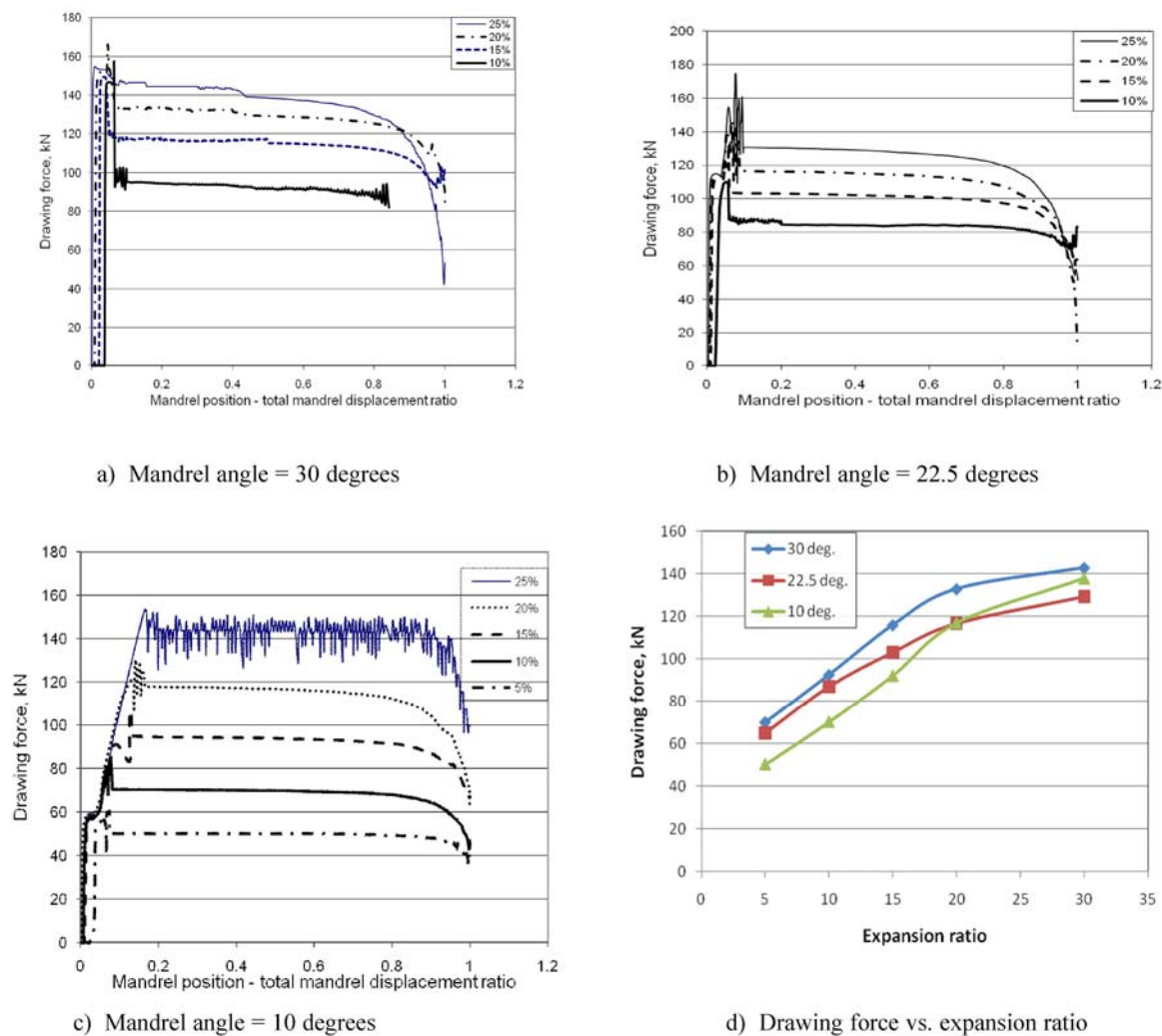


Figure 2. Drawing force required for tube expansion for various expansion ratios and mandrel angles

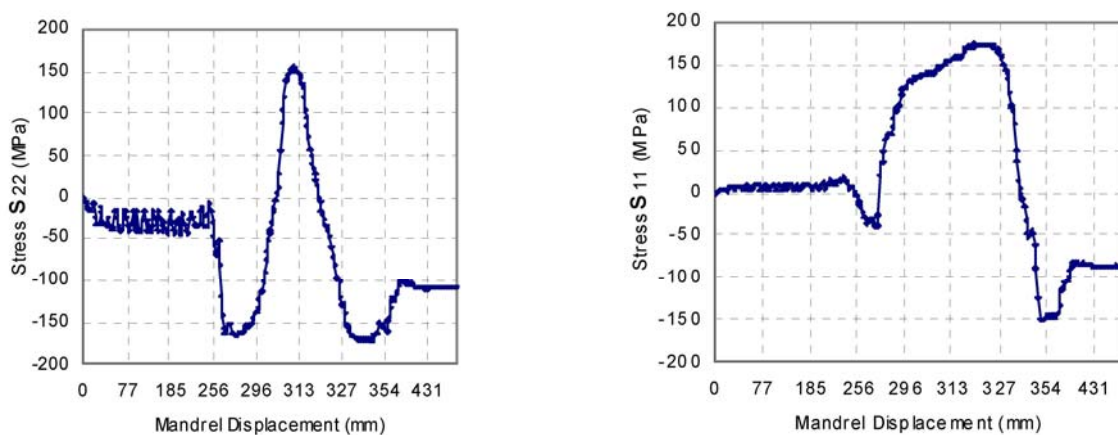


Figure 3. Tangential stresses (S_{22} and S_{11}) versus mandrel position for an expansion ratio of 5%, mandrel angle of 10° , and when $d/t = 1.5$

Figures 6 and 7 show the behavior of the SCF K_{max} as a function of the ratio of the hole-diameter-to-tubular wall thickness at both locations for an expansion

ratio of 5% and three different mandrel angles. K_{max} decreases for both cases as the ratio of d/t and the mandrel angle increase. This decrease is mainly attributed

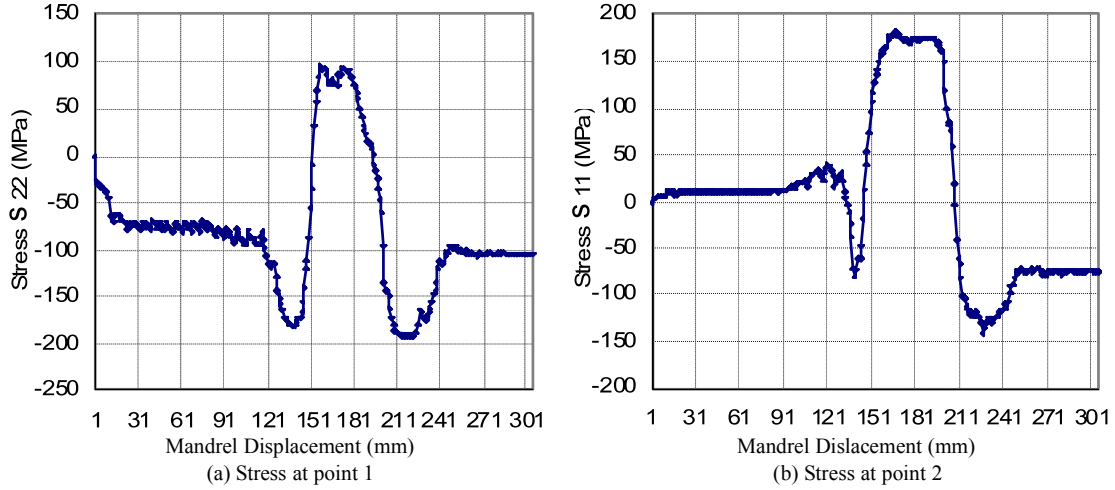


Figure 4. Tangential stresses versus mandrel position for an expansion ratio of 25%, mandrel angle of 30°, and when $d/t = 0.6$

Table 1. SCF for a mandrel angle $\beta = 10^\circ$

| % Expansion | K_{\max} |
|-------------|--|
| 5 | $K_{\max}^{5\%} = 154.66 - 575.94\left(\frac{d}{t}\right) + 1658.61\left(\frac{d}{t}\right)^2 - 3265.48\left(\frac{d}{t}\right)^3$ $+ 4103.53\left(\frac{d}{t}\right)^4 - 3101.09\left(\frac{d}{t}\right)^5 + 1273.97\left(\frac{d}{t}\right)^6 - 217.46\left(\frac{d}{t}\right)^7$ |
| 10 | $K_{\max}^{10\%} = 135.88 - 527.60\left(\frac{d}{t}\right) + 1347.41\left(\frac{d}{t}\right)^2 - 2047.10\left(\frac{d}{t}\right)^3$ $+ 1700.31\left(\frac{d}{t}\right)^4 - 625.15\left(\frac{d}{t}\right)^5 + 1.98\left(\frac{d}{t}\right)^6 + 39.08\left(\frac{d}{t}\right)^7$ |
| 15 | $K_{\max}^{15\%} = 98.10 - 366.10\left(\frac{d}{t}\right) + 776.64\left(\frac{d}{t}\right)^2 - 680.64\left(\frac{d}{t}\right)^3$ $- 253.11\left(\frac{d}{t}\right)^4 + 950.84\left(\frac{d}{t}\right)^5 - 658.20\left(\frac{d}{t}\right)^6 + 150.60\left(\frac{d}{t}\right)^7$ |
| 20 | $K_{\max}^{20\%} = 113.26 - 616.24\left(\frac{d}{t}\right) + 2079.63\left(\frac{d}{t}\right)^2 - 4156.90\left(\frac{d}{t}\right)^3$ $+ 4986.06\left(\frac{d}{t}\right)^4 - 3533.69\left(\frac{d}{t}\right)^5 + 1364.66\left(\frac{d}{t}\right)^6 - 221.20\left(\frac{d}{t}\right)^7$ |
| 25 | $K_{\max}^{25\%} = 92.74 - 561.71\left(\frac{d}{t}\right) + 1878\left(\frac{d}{t}\right)^2 - 4127.41\left(\frac{d}{t}\right)^3$ $+ 5454.66\left(\frac{d}{t}\right)^4 - 4228\left(\frac{d}{t}\right)^5 + 1764.6\left(\frac{d}{t}\right)^6 - 305.08\left(\frac{d}{t}\right)^7$ |

to the increase of the nominal stress σ_{nom} and the decrease of the maximum stress σ_{max} as of the ratio of d/t increases.

It is worth mentioning that the SCF based on σ_{max} decreases as the expansion ratio increases from 5 to 25% which is also attributed to the decrease of nominal stress as the expansion ratio increases from 5 to 25%.

4.1 Semi-analytical Formulations of Stress Concentration

This section aims to develop expressions for the SCFs as functions of the parameters d/t , β , and e used in this study. Table 1 shows expressions for the stress concentration factor K_{\max} in terms of hole-diameter-to-tube-wall thickness for one set of data.

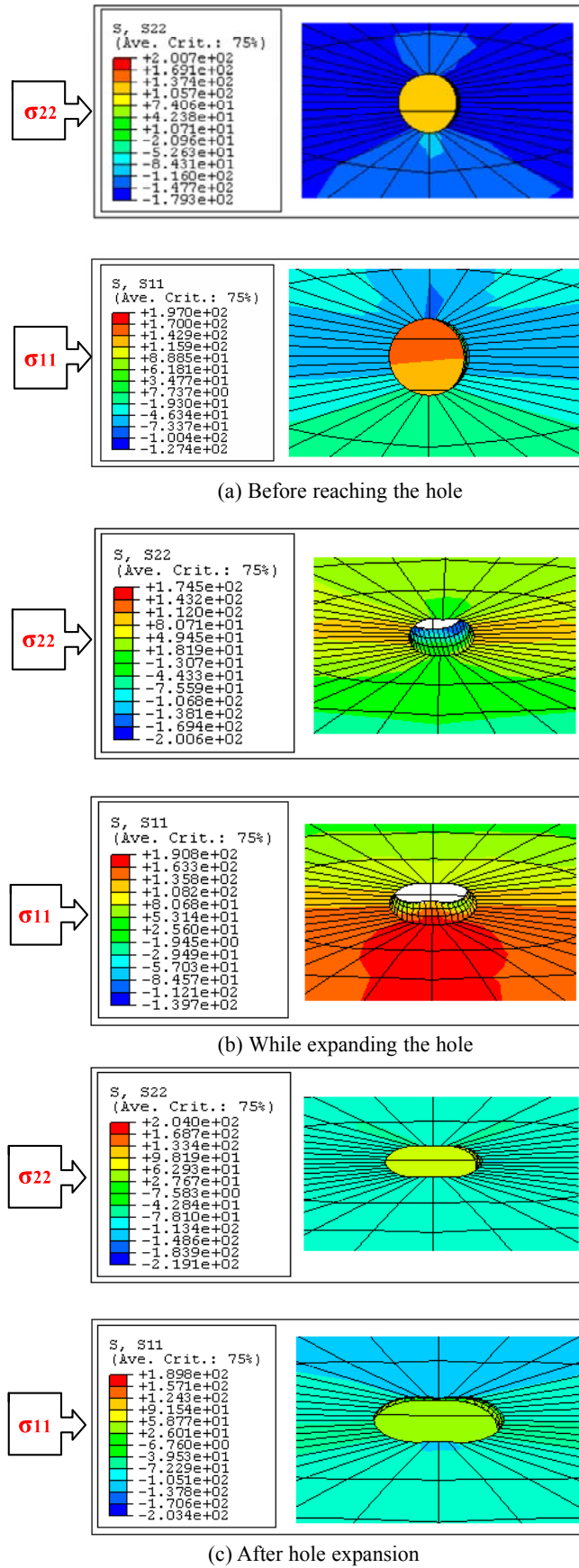


Figure 5. Stress contours and shapes of the hole during the complete expansion process

Stress Concentration Factor of Expanded Aluminum Tubes Using Finite Element Modeling

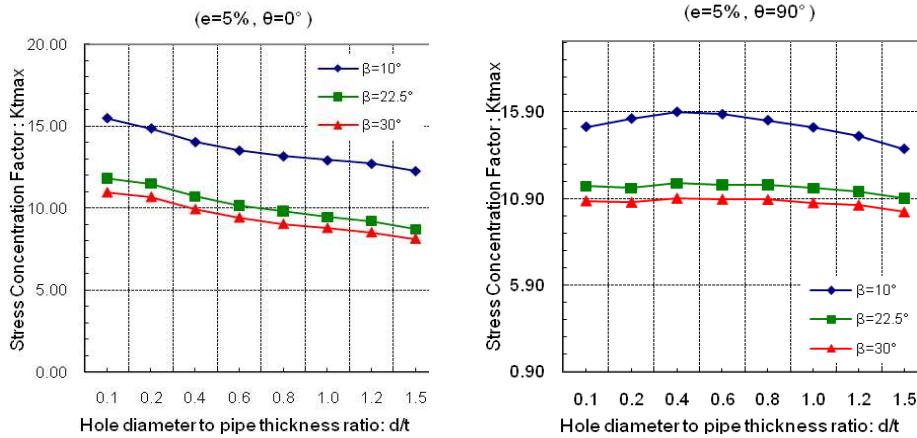


Figure 6. SCF as a function of the hole-diameter-to-tube-thickness ratio for 5% expansion ratio and mandrel angles of 0 and 90 degrees

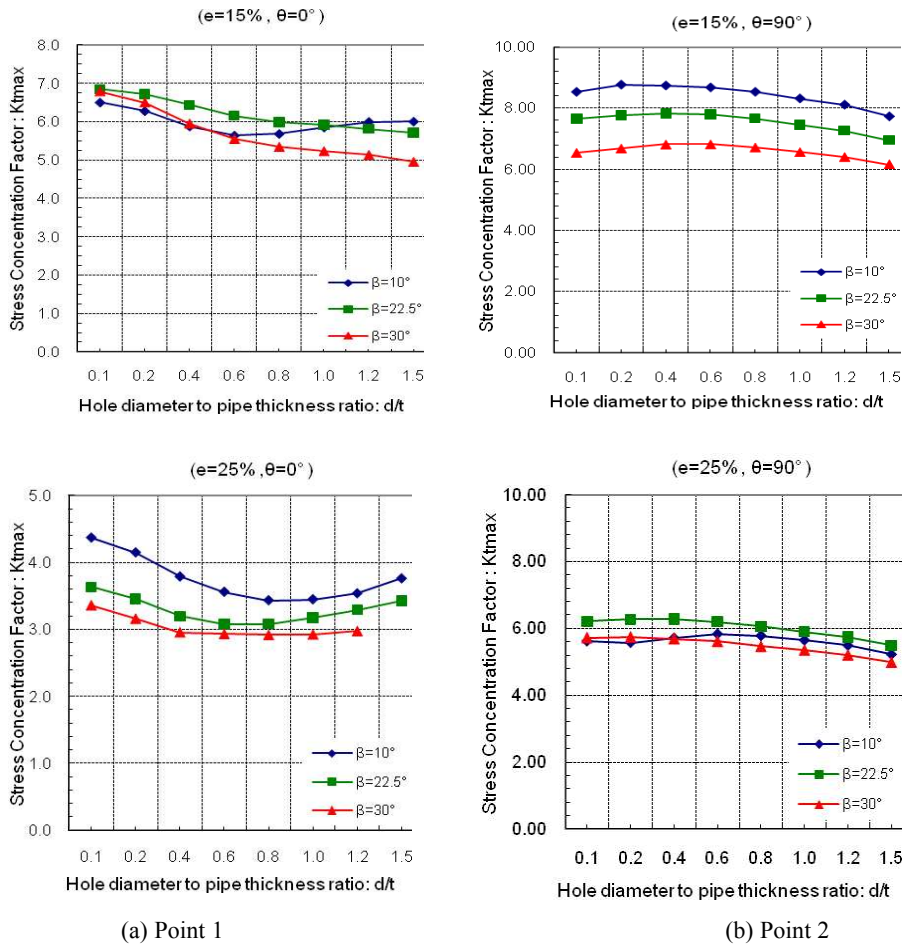


Figure 7. SCF as a function of hole-diameter-to-tube-thickness ratio, expansion ratios and mandrel angles

These seventh-order polynomials are valid within the range used in this study ($0.1 \leq d/t \leq 0.15$). To develop such relations, the Lagrange interpolation method, which is an efficient numerical technique, was used. The advantage of this technique is that the

data set points need not be arranged in any particular order as long as they are mutually distinct. The analysis started with a data set consisting of one set of either parameter (d/t, β , or e) and their corresponding values of (K_{tmax}) for a well-determined case. Several cases

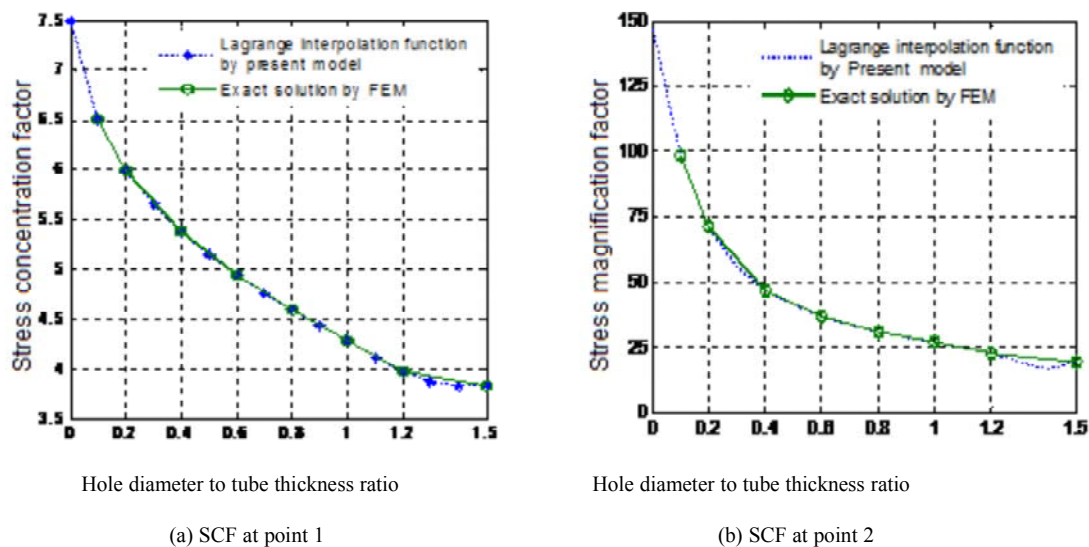


Figure 8. SCF K_{max} versus hole-diameter to tube-thickness ratio for an expansion ratio of 5% and mandrel angle of 22.5°

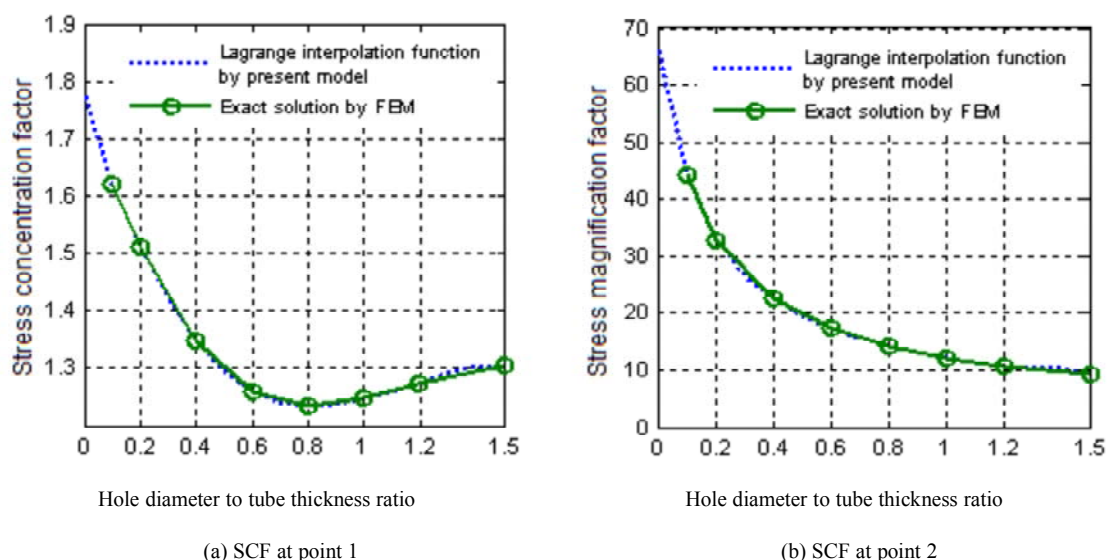


Figure 9. SCF K_{max} versus hole-diameter to tube-thickness ratio for an expansion ratio of 25% and mandrel angle of 22.5°

were studied to determine the effect of each parameter on the SCF. Similar expressions can be developed for other parameters. Figures 8 and 9 show a comparison between the finite element results and the developed semi-analytical model for K_{max} for different expansion ratios at points 1 and 2, respectively. Both figures show good agreement between the finite element results and the developed model. Figure 8 shows that

the stress magnification factor is plotted at point 2 due to higher values of stress. The stress at point 2 experienced a significant change in value because the stress state changed from compression (pre-mandrel position) to tension (post-mandrel position) as the mandrel traveled along the tube during expansion.

A general expression of the maximum K_{max} SCF for the various parameters used in this study $\left(e, \frac{d}{t}, \frac{\beta}{\beta_0}\right) \in E^1 \times E^2 \times E^3$ was developed and takes the following form:

$$K_{t_{max}} \left(e, \frac{d}{t}, \frac{\beta}{\beta_0} \right) = \frac{1}{3} \left[\left(K_{t_{max}} \right)_{e, \beta / \beta_0} \left(\frac{d}{t} \right) + \left(K_{t_{max}} \right)_{e, d/t} \left(\frac{\beta}{\beta_0} \right) \right] + \left(K_{t_{max}} \right)_{d/t, \beta / \beta_0} (e) \quad (2)$$

$$\begin{aligned} \left(K_{t_{max}} \right) \left(e, \frac{d}{t}, \frac{\beta}{\beta_0} \right) = & \frac{1}{3} \left(a_0 + a_1 \left(\frac{d}{t} \right) + a_2 \left(\frac{d}{t} \right)^2 + a_3 \left(\frac{d}{t} \right)^3 + a_4 \left(\frac{d}{t} \right)^4 + a_5 \left(\frac{d}{t} \right)^5 \right) \\ & + a_6 \left(\frac{d}{t} \right)^6 + a_7 \left(\frac{d}{t} \right)^7 + b_0 + b_1 \left(\frac{\beta}{\beta_0} \right) + b_2 \left(\frac{\beta}{\beta_0} \right)^2 + c_0 \\ & + c_1 (e) + c_2 (e)^2 + c_3 (e)^3 + c_4 (e) \end{aligned} \quad (3)$$

Equation (3) represents a semi-analytical formulation of the stress concentration factors. It is worth to note that this equation is applicable for $\left(e, \frac{d}{t}, \frac{\beta}{\beta_0}\right) \in E^1 \times E^2 \times E^3$ and is valid for any combination of data within the range of values for $(d/t, \beta, e)$ used in this study. The constants of the polynomials can be easily determined for each set of data.

5. Conclusions

The results from three-dimensional elastic perfectly-plastic finite-element analyses were presented to compute the SCFs around circular holes in perforated tubes subjected to a compressive expansion process. Over 120 finite element models were run in order to study the effect of the parameters d/t , β , and e on the SCFs. It was found that both SCFs were higher at point 2 (90° location) indicating that failure might originate at this location. In addition, the results showed that the SCF decreased as the hole-diameter-to-tube-thickness ratio and mandrel angle increased. Moreover, generalised semi-empirical relations of both SCFs in terms of d/t , β , and e were developed using the Lagrange interpolation method. These expressions can reproduce any of the finite element results with the range of the parametric values undertaken in this study.

References

- Chitwood GB, Eisinger NC, Puckett BC (2005), Corrosion resistant and long-term reliability of super-austenitic alloy 27-7MO for use as expandable tube. SPE95094. SPE International Symposium on Oilfield Corrosion, Aberdeen, United Kingdom.
- Dennis ST, Palazotto AN (1990), Static response of a cylindrical composite panel with cutouts using a geometrically nonlinear theory. Journal of American Institute of Aeronautics and Astronautics 28(6):1082-1088.
- Pilkey WD (1997), Peterson's stress concentration factors. 2nd Edition, Wiley Interscience, John Wiley and Sons, ISBN: 978-0-471-53849-3.
- Steele CR, Steele ML, Khathlan A (1986), An efficient computational approach for a large opening in a cylindrical vessel. ASME Journal of Pressure Vessels Technology 108(4):436-443.
- Tan SC (1994), Stress concentrations in laminated composites. CRC Press, Taylor and Francis Group, USA.
- Toubal L, Karama M, Lorrain B (2004), Stress concentrations in a circular hole in composite plate. Composite Structure 68:31-36.
- Van DP (1965), Stress about a circular hole in a cylindrical shell. Journal of American Institute of Aeronautics and Astronautics 3:1733-1742.
- Xue MD, Deng Y, Hwang KC (1991), Some results on the analytical solution of cylindrical shells with large openings. ASME Journal of Pressure Vessels Technology 113(2):291-308.